Screened hybrid and self-consistent GW calculations of cadmium/magnesium indium sulfide materials

Melissa J. Lucero, Irene Aguilera, Cristian V. Diaconu, Pablo Palacios, Perla Wahnón, and Gustavo E. Scuseria

Phys. Rev. B **83**, 205128 — Published 25 May 2011

DOI: 10.1103/PhysRevB.83.205128

Screened Hybrid and Self-Consistent GW Calculations of Cadmium/Magnesium Indium Sulfide Materials

Melissa J. Lucero,[1] Irene Aguilera,[2] Cristian V. Diaconu,[1]
Pablo Palacios,[2,3] Perla Wahnón,[2] and Gustavo E. Scuseria[1,4]

[1] *Department of Chemistry, Rice University, Houston, TX 77005-1892, USA*
[2] *Instituto de Energía Solar and Departmento Tecnologías Especiales, ETSI Telecomunicatión, UPM, Ciudad Universitaria, Madrid 28040, Spain*
[3] *Física y Química Aplicadas a la Técnica Aeronáutica, E. de Ingeniería Aeronáutica y del Espacio, UPM, Ciudad Universitaria, Madrid 28040, Spain*
[4] *Physics & Astronomy Department, Rice University, Houston, Texas 77005-1827, USA*

The cadmium and magnesium indium sulfides are medium-gap semiconductors demonstrating a propensity to form intermediate band materials when doped with transition metals. The inherent structural diversity exhibited by $M^{+2}In_2S_4$ thiospinels and related AB_2X_4 compounds often preclude definitive experimental determination of the band gap width and type of transition. Employing a series of traditional semi-local functionals (LDA, PBE, TPSS) and the screened hybrid HSE, band gaps, projected densities of states and band structures are calculated for the normal, full inverse and intermediate configurations of $[Cd/Mg]_8In_{16}S_{32}$. Band structures and band gaps are also obtained via self-consistent many-body methods, using the static Coulomb-hole and screened exchange approximation to *GW* as a starting point for perturbative G_0W_0 calculations. Comparison to experiment indicates that HSE provides an accurate, computationally-efficient and relatively rapid means for predicting band gap properties in spinel-type photovoltaic materials.

PACS numbers: 71.15.Mb, 71.20.Nr, 78.20.Bh

I. INTRODUCTION

Photovoltaic cells containing intermediate band (IB) materials are capable of efficiently absorbing photons over a broad range of the solar spectrum. An intermediate band optimally situated between the valence and conduction bands can result in electron promotion using two photons with a combined energy expenditure *smaller* than the typical one photon electronic excitation across the analogous semiconductor gap, boosting ideal efficiencies from 40.7%[1] to 63.1%.[2] Rapid prescreening of semiconductors with ca. 2-3 eV band gaps will facilitate selection, suggest modification, and expedite fabrication of IB-forming, doped semiconductors.

To date, the majority of solid state computational studies employ semilocal[3] exchange correlation functionals (*e.g.,* the LDA, GGA or meta-GGA variants) which consistently fail to reproduce experimental band gaps despite the development of more sophisticated approximations.[4] Intermediate band photovoltaics are formally metallic, yet still closely resemble the undoped parent semiconductors which tend to have underestimate bands gaps on the order of 1 eV.[5–9]

Fortunately, more accurate results, comparable to those of full, self-consistent (sc) GW calculations[10] are accessible, at reduced computational cost, by employing the Coulomb-hole and screened exchange (COHSEX)[11,12] approximation. The COHSEX approximation accounts from statically-screened exchange and correlation in the form of the classical interaction between and additional point charge in the system and the surrounding polarization cloud that this additional charge induces. The static COHSEX result is then augmented with dynamic effects through a perturbative G_0W_0 calculation. The main effects neglected by this scheme are the excitonic and polaronic effects.

The scCOHSEX+G_0W_0 (scGW) scheme has been successfully applied to a wide range of materials,[11,13–16] yielding *fundamental* band gaps (as opposed to the smaller *optical* gaps) and band structures, often in good agreement with experiment. Nevertheless, when applied to IB materials doped with high concentrations of transition metals, even these many-body corrections become prohibitively expensive for all but the smallest systems.[17]

Other well-established, less CPU-intensive corrections are also unsuitable for modeling transition metal-doped IB materials: perturbative G_0W_0 after LDA cannot accurately address the influence of populated *d*-orbitals on band gaps,[11,18] while DFT+U methods require system-dependent parameters that are unknown for novel materials. It is worth nothing that the screened short-range Hartree-Fock exchange interactions in the hybrid functional of Heyd, Scuseria and Ernzerhof[19–21] (HSE) are reminiscent of the role that the Hubbard on-site repulsion U plays in DFT+U. However, unlike +U methods, HSE can allocate a unique effective "U" to different orbital interactions. In fact, a recent paper[22] advocates the use of HSE to determine U when experimental information is lacking and the need to reduce computational effort surmounts the desire for increased prediction quality. Significantly, HSE *alone* produces semiconductor band gaps and lattice parameters in excellent agreement with experiment,[19,23] without requiring multiple calculations, perturbative adjustments or material-dependent parameters – and at significantly reduced cost relative to many-body corrections.[13,14,24–26]

Recently, the $M^{+2}In_2S_4$ semiconductors containing Mg and Cd, garnered considerable attention due to their potential application in high-efficiency solar cells.[6,27] Spinel-type chalcogenides are capable of adopting a variety of related crystalline forms,[28] a consequence of the AB_2X_4 lattice affording the anions freedom to expand or contract around their fractional coordinates, thus allowing facile accommodation of a wide range of cation sizes, while maintaining overall symmetry. The literally hundreds of known spinels are classified according to the 24 occupied interstices of the *fcc* lattice (defined by X). By convention, the eight smaller, usually divalent cations occuping T_d holes are designated A, while the remaining sixteen, typically higher-valent B cations reside in O_h holes[29] yielding crystallographic unit cells of composition $A_8B_{16}X_{32}$, where X=O, S, Se, or Te.

The limiting designations[30] for cation occupancy in spinel structures are (a) *normal*, with all A cations filling T_d sites, and all B cations in O_h holes or (b) *full inverse*, in which $A = B$ for occupied O_h sites, forcing half of the B cations into T_d holes. The term *partial inverse* describes the spectrum of intermediate spinel structures, $x = A_{1-x}B_x[A_xB_{2-x}]X_4$, where brackets denote O_h sites. Thus defined, the degree of inversion, x, ranges from 0 (normal) to 1 (full inverse), with $x = \frac{2}{3}$ representing a fully stochastic system.

II. COMPUTATIONAL METHODS

Density Functional Calculations. Electronic structure calculations were performed using the periodic boundary-condition code[31–33] within the GAUSSIAN suite of programs.[34] Data analysis and visualization were performed using GaussView[35] and VMD.[36]

Gaussian basis sets modified for solids are provided in the Supplementary Material[37] and are of the following quality: Mg: 8-511G (all-electron); S: 6-311G*(all-electron); Cd: 6-311G (all-electron); In: 4*s*4*p*2*d* (ECP, modified.) Unless otherwise noted, initial geometries are the conventional, crystallographic unit cells ($Fd\bar{3}m$, 227), downloaded as CIF files from the ICSD,[38] The 56-atom crystallographic unit cells are optimized in redundant internal coordinates[39] with 36 **k** points on a 4×4×4 mesh for the reciprocal space integration. The 14-atom primitive cells are optimized similarly, but employ 112 **k** points on a 6×6×6 mesh.

Reported band gaps and related properties for fully-relaxed (lattice parameters and geometries) periodic systems were obtained using three semilocal and one screened hybrid functional to create a series of increasingly sophisticated exchange-correlation approximations. Specifically, we compare the Local Spin Density Approximation, LSDA[40] (with SVWN5[41]), the generalized gradient approximation (GGA) corrected functional of Perdew, Burke and Enzerhof[42,43] (PBE), the meta-GGA functional of Tao, Perdew, Staroverov and Scuseria[44] (TPSS) and the non-local Heyd-Scuseria-Enzerhof[45] screened hybrid functional, (HSE).

Many Body Calculations. All many-body calculations were performed on 14-atom cells using the plane-wave based code ABINIT.[46] For the COHSEX and G_0W_0 calculations,[47] a basis set of ca. 25,000 plane waves was required for convergence. A Monkhorst-Pack **k**-point mesh of 3×3×3 was used to sample the Brillouin Zone. Norm-conserving pseudopotentials[48] were generated with the *fhi*98*PP* code,[49] accounting for *semicore states* (*e.g.,* the 4*s*4*p*4*d* of In) explicitly in the valence, following Hybertsen.[50] Details of the pseudopotential generation procedure can be found in the Supplementary Material.[37] The plasmon-pole model[51] is used for G_0W_0 calculations and COHSEX wavefunctions are represented on a restricted LDA basis set as proposed by Bruneval.[11] All scGW calculations start from relaxed LDA-optimized structures: normal $Cd_2In_4S_8$: a_o = 10.775 Å, normal $Mg_2In_4S_8$: a_o = 10.682 Å, full inverse $Mg_2In_4S_8$: a_o = 10.634 Å.

III. CADMIUM INDIUM SULFIDE

Numerous applications, particularly in photovoltaics and LEDs,[52–54]render cadmium indium sulfide an extremely well-studied thiospinel, generally accepted to crystallize in a *normal* structure, with $x \approx 1$, although studies involving partial inverse structures and mixed crystals have been reported.[55,56] DFT calculations of normal $CdIn_2S_4$ were performed on the conventional 56-atom crystallographic unit cells ($Fd\bar{3}m$, 227), as well as the 14-atom primitives. The inverse ordering is modeled using only the primitive cells.

A. Cd Normal Spinel Structure

Measured band gaps are on the order of 2.1-2.7 eV.[52,57–66] A rather broad range of band gaps is also observed for the related spinel-type transparent conducting oxides (TCOs) $CdIn_2O_4$, $E_g = 2.67 - 3.24$[67] and Cd_2SnO_4, $E_g = 2.06 - 3.00$.[67,68] Comparison of bulk and thin film specimens of the $Cd_{1+x}In_{2-2x}Sn_xO_4$ solid solution demonstrates that the optical gaps for thin films are significantly larger than for bulk samples,[69] this difference most likely arising from a Burstein-Moss shift.[70] Furthermore, the gap narrows as the cation ordering becomes more inverted,[71] a consequence of the order-disorder phenomena discussed in Section IV. Note that there are many documented *larger* lattice constants than the commonly cited $a_o = 10.797$. Lee *et al.*[60] report that the $CdIn_2S_4$ a_o varies according to the method of crystal growth, ranging from 10.838-10.860 Å, rather larger than the 10.797 Å reported by Hahn.[72] Thus, the band gap widths for these systems are affected by dimensionality and degree of inversion, which is dependent upon method of synthesis: films have larger gaps and any reaction condition that facilitates inversion, results in lower

gaps.

As indicated in Table I, the three semilocal functionals underestimate the gap for the normal spinel by at least 1 eV, as expected, while the screed hybrid HSE provides band gaps close to that of experiment at 2.33 eV, tending toward the bottom of the reported experimental band gaps. There is also an experimental lack of consensus (see Ref. 73 and references therein) regarding the *nature* of the transition. However, all four functionals predict an *indirect* transition that is ca. 10 meV lower in energy than the for the direct path, perhaps indicating that this minor energy difference is somehow related to the general disagreement regarding the type of band gap. (The common practice of reporting only one decimal place induces a coalescence of theoretical gaps, thus forcing inference of a *direct* gap.) This vanishingly small ΔE is not unique: β-In_2S_3, also has experimental band gaps ranging from 2-3 eV in magnitude with disputed indirect/direct transitions typically varying by ca. 10 meV.[74] Note that the β-In_2S_3 structure can be considered a parent of the many indium thiospinels, and it is often described as a quasi-quaternary defect spinel with cationic vacancies in the T_d sites ordered along the c-axis.[75]

TABLE I. Normal and Full Inverse $CdIn_2S_4$: Functional Dependence of Band Gap (eV) and Lattice Parameters (Å)

Functional	LDA		PBE		TPSS		HSE	
Nature of Gap	E_i	E_d	E_i	E_d	E_i	E_d	E_i	E_d
Normal	$Cd_8In_{16}S_{32}$			56-atom cell				
Experiment	**2.2-2.7**[a]		**a_o = 10.797**[b]					
a_o	10.840		11.106		11.073		11.000	
Band Gap[c]	1.34	1.44	1.21	1.28	1.52	1.60	2.33	2.41
rlx→HSE_{sp}[d]	2.14	2.25	2.13	2.21	2.19	2.28	—	
Full Inverse	$Cd_2In_4S_8$			14-atom cell				
a	7.671		7.861		7.835		7.776	
b	7.722		7.909		7.883		7.841	
c	7.656		7.842		7.813		7.763	
Band Gap[c]	0.21	0.22	0.13	0.14	0.37	0.40	1.19	1.23
rlx→HSE_{sp}[d]	1.39	1.42	1.02	1.06	1.08	1.11	—	

[a] Refs. 52, 57–66
[b] ICSD ID 300725[72]
[c] Fully-relaxed geometry and forces.
[d] Relaxed using LDA/PBE/TPSS then HSE energy calculation.

The 0 K lattice parameters predicted by LDA most closely resemble measured values, yet the HSE-relaxed geometry, with a slightly larger volume, has a band gap in much better agreement with experiment. In fact, while LDA geometries are generally considered to be better for semiconductors, the UV photoemission spectra of $CdIn_2S_4$ and related spinels exhibit little sensitivity to small crystallographic deviations.[76] Full-relaxation using each of the semilocal functionals, followed by HSE single point energy calculations is summarized in the "Rlx→HSE_{sp}" row of Table I. All relaxed lattices, with a_o varying from experiment by 4-30 pm, result in gaps close to – or within – the experimental range, clearly illustrating the profound effect that the introduction of non-local Hartree-Fock-type exchange has on band width.

Moreover, the HSE single point energy of the LDA-relaxed structure, with a gap of 2.14 eV, and the HSE-relaxed gap of 2.33 eV are at the bottom of the experimental range, which correctly corresponds to bulk,[58,59] rather than thin film[52,53] band gaps. Indeed, a recent study of hierarchical nanostructured $CdIn_2S_4$ produced at low temperatures using different methods result in multiple morphologies yet the band gaps were constrained to a narrow range of 2.23-2.27 eV.[77]

Admittedly, evaluation of Hartree-Fock exchange is computationally expensive for *any* hybrid functional. This potential bottleneck may be surmounted by first performing a full relaxation with a less-expensive functional, followed by a single point energy calculation using HSE. This simple shortcut yields more accurate band gaps and would work equally well for *any* functional considered to produce superior lattice parameters, whether traditionally semilocal or next-generation, designed specifically for solids, *e.g.,* HSEsol.[78] This procedure should prove quite useful, particularly for studies of formation energies of interstital defects,[79] defect transition levels[80] (HSE performs particularly well for both) or any investigation requiring large supercells. Moreover, this shortcut is possible in any software package with an implementation of HSE.

B. Cd Full Inverse Spinel Structure

The experimentally unobserved full inverse structure (bottom section, Table I) like the normal spinel, also has a marginally indirect band gap, predicted to have a width of 0.1-04 eV by all functionals except HSE, which produces a somewhat larger, 1.2 eV gap. The HSE single point energies of structures relaxed using semilocal functionals also show an increased in gap, with the indirect transition favored, again, by only meV. Notably, the analogous spinel oxide, $CdIn_2O_4$, was also calculated to have a smaller band gap in the inverse spinel structure.[81] HSE thus provides an interesting prediction of a 1.2-1.4 eV band gap should such a structure be isolated.

C. Densities of States

The $Cd_8In_{16}S_{32}$ normal spinel projected density of states (PDOS) are plotted for each functional in Figure 1. The In 5s- (blue) and S 3p-orbitals (yellow) dominate the conduction band, while the primary contribution to the valence band is almost exclusively S 3p-orbital. This pattern is strikingly similar to that observed for β-In_2S_3, which has a gap of around 2.1 eV.[82,83] The Cd 5s contribution is minimal in both the top of the valence and bottom of the conduction bands, demonstrating that metal insertion into the β-In_2S_3 manifold produces more significant structural consequences (ordered defect spinel → normal spinel) than for electronic prop-

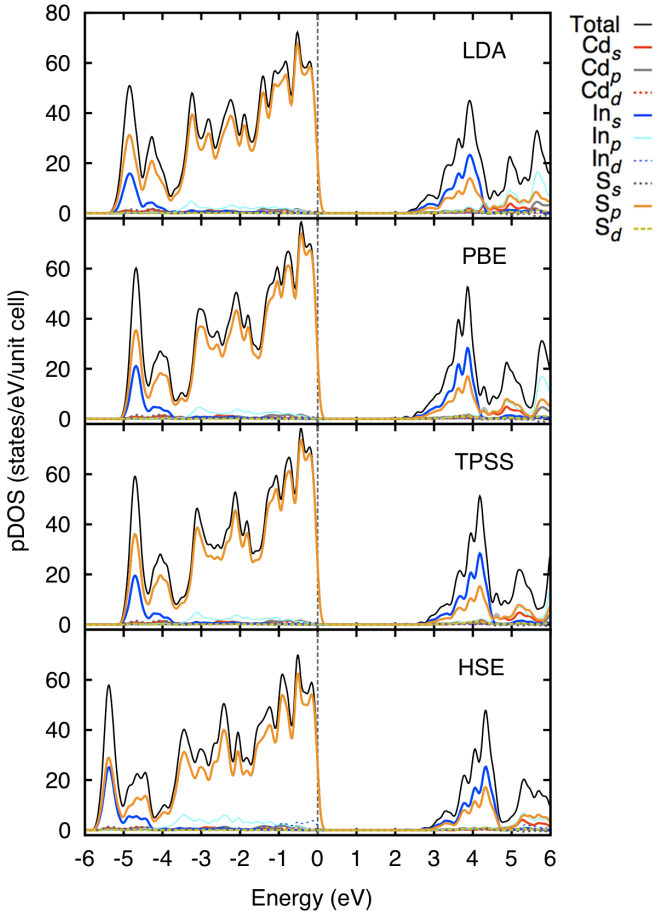

FIG. 1. Projected density of states for $Cd_8In_{16}S_{32}$ as a **Normal** spinel structure, calculated with LDA, PBE, TPSS and HSE. The Fermi level is indicated by the dashed black line at $E = 0$. The top of the valence band does not terminate exactly at zero due to a 10 meV Gaussian line-broadening.

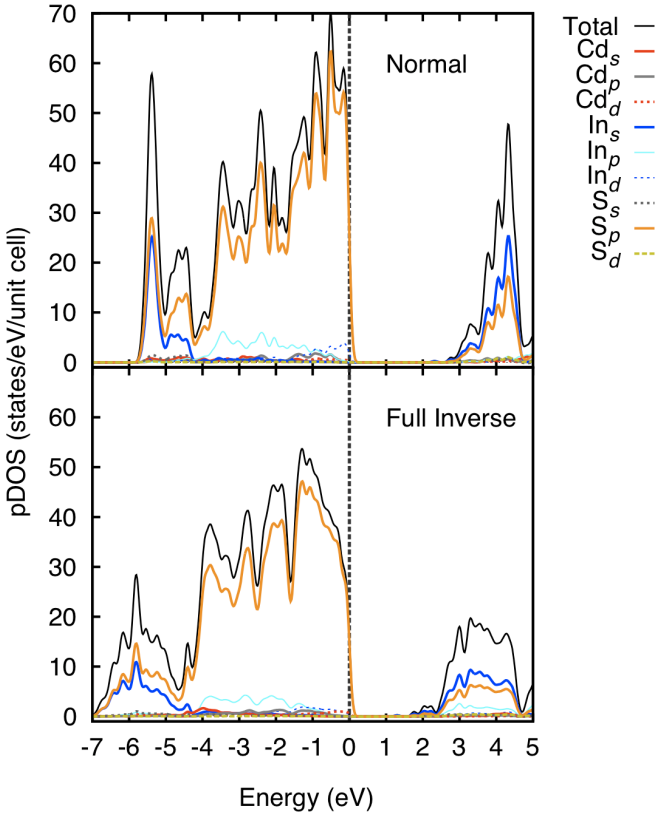

FIG. 2. The HSE projected density of states for $Cd_8In_{16}S_{32}$ in **Normal** (top) and **Full Inverse** (bottom) spinel structures. The Fermi level is indicated by the dashed black line at $E = 0$. The top of the valence band does not terminate exactly at zero due to a 10 meV Gaussian line-broadening.

erties relevant to the band gap. As the exchange correlation approximations improve, LDA → TPSS, a clear blue shift is observed for the conduction band, which dramatically increases upon introduction of non-local Hartree-Fock exchange (HSE). In contrast, very little of interest transpires in the valence band, which is somewhat wider for HSE than the semilocal functionals. The HSE band resembles that for LDA, but has more structure and a slightly extended (ca. 0.2-0.3 eV) low energy tail.

The transition from normal to full inverse spinel structures results marked decrease in the predicted band gaps – from 2.3 to 1.2 eV – and both the valence and conduction bands broaden and change morphology, as is illustrated in Figure 2. Further, a small band on the edge of the low energy tail of the conduction band appears in both spinels, which is discernible in the bottom of Figure 2, between 1-2 eV (2-3 eV in the normal spinel). Enlargements of these regions are depicted in Figure 3, in order to facilitate comparison of the HSE PDOS. While the In 5*s*-orbitals predominate in both cases, the enlargements indicate that this small, almost isolated, feature closely resembles the larger section of the conduction band, yet the relative contributions of the sulfur and cadmium orbitals change. In the normal spinel, Figure 3 (a) and (c), the sulfur 3*s*- 3*p*- and Cd 5*s*-orbital contributions are nearly identical, while in the full inverse structure, Figure 3 (b) and (d), the sulfur 3*s* contribution increases as does that of the In 4*d*-orbitals, which were not present in the tail of the normal spinel (c) at all.

IV. MAGNESIUM INDIUM THIOSPINELS

While observed in natural spinel, $MgAl_2O_4$, the normal structure is not adopted by many synthetic Mg-containing spinel oxides.[84,85] As already discussed, this dependence of configuration upon method of formation/synthesis is also observed for many thiospinels, including those with A = Mg[86] and is consequence of the oxygen or chalcogenide anions forming a highly-adaptable *fcc* structure, allowing a wide range of cations to not only occupy, but move in between the T_d and O_h holes. This structural mobility is influenced by the chemical composition, but is more sensitive to the ordering of occupied holes, which, in turn, varies according

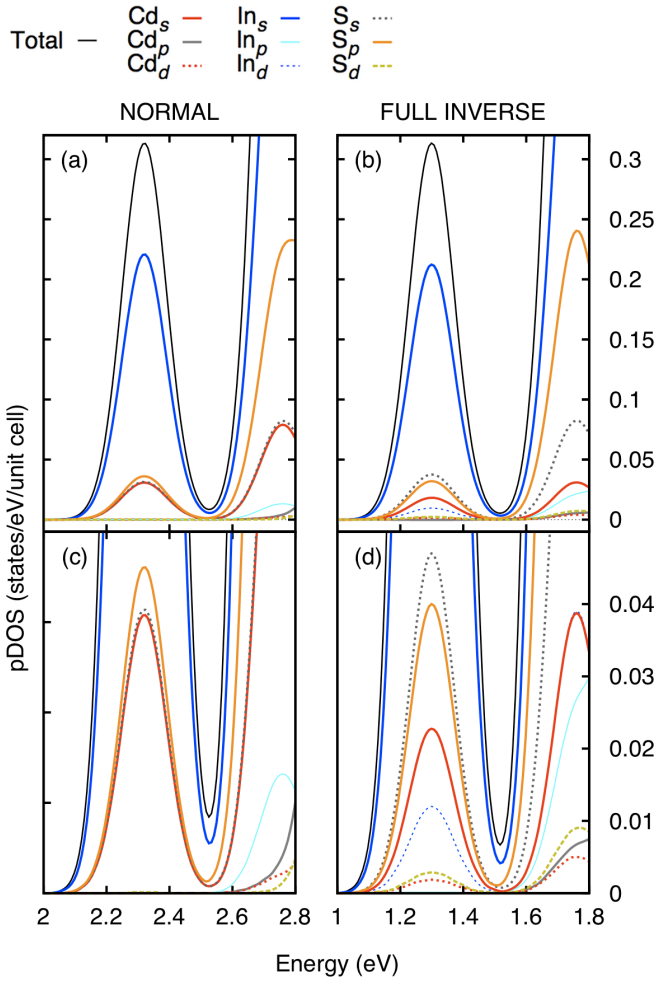

FIG. 3. Enlargement of the low energy region in the conduction bands of the HSE projected density of states for $Cd_8In_{16}S_{32}$ adopting **Normal** (left) and **Full Inverse** (right) spinel structures. The top figures (a) and (b) highlight the similar band shapes, but somewhat different population densities, while the increased zoom in the bottom plots (c) and (d) further illustrate the disparate contributions from the relevant S, Cd and In orbitals as the spinel structure is inverted.

to cation size, electrostatic interactions, structure defects and temperature.[87,88] Experimental determination of the *ground state* cation distributions is thus non-trivial, particularly since the high temperatures requisite for most older spinel syntheses mimic the formation conditions of the natural minerals known to form metastable crystalline states,[89] and consequent adherence to Ostwald's Rule.[90] At lower temperatures, thermal equilibrium is also difficult to obtain due to very low diffusion rates.[91]

Not surprisingly, several *order-disorder* phenomena[92] have been recognized in spinels. The normal spinels generally exhibit long-range, non-convergent order-disorder behavior, in which the extent of inversion changes continuously without a phase transition, while inverse spinels exhibit two types of order-disorder behavior (1) an ordered inverse → disordered inverse first-order transition stabilized by configurational entropy-associated cation exchange in O_h sites or (2) a non-convergent disordered inverse to another disordered state stabilized entropically by cation exchange in both T_d and O_h sites.[93]

The stability of the normal vs. inverse structures, for $Cd/MgIn_2S_4$, assuming low temperature thermal equilibrium is presented in Table II. From a 0 K perspective, the Cd system makes sense thermodynamically, implying that a normal structure should predominate, assuming thermal equilibrium is achieved. Recall from Section III that experimentally, normal (or close to normal) structures are observed and a full inverse analog has not been isolated.

TABLE II. $M^{2+}In_2S_4$ Relative Energies by Type (kcal/mol)

Functional (FNL)	LDA	PBE	TPSS	HSE
Spinel Type				
$MgIn_2S_4$				
Normal	0.00	0.00	0.00	0.00
Partial Inverse	4.60	3.27	3.02	3.37
Full Inverse	4.13	2.67	2.42	2.15
$CdIn_2S_4$				
Normal	0.00	0.00	0.00	0.00
Full Inverse	17.01	17.00	17.49	16.57

For the Mg thiospinels, the energy preference between either inverse ordering and the normal structure is significantly reduced. This is not surprising, as both $MgIn_2S_4$ and its oxide equivalent, $MgIn_2O_4$, are observed to adopt some form of inverse structure.[86] The partial inverse configuration is calculated to be *less* stable than the full inverse, yet experimentally, a fully inverse structure has not been isolated. Nevertheless, $MgGa_2O_4$, a spinel with an experimental degree of inversion similar to our partial inverse structure (ca. 0.84),[94] was shown via finite temperature MC calculations,[91] to prefer an inverse-type structure at RT, strongly implying that synthetic $MgIn_2S_4$ is subject to some form of order-disorder behavior. Recent specialized models[95] and finite temperature simulations[96] demonstrate that predicting whether or not whether a normal or inverse-type ordering scheme will predominate in the 0-278 K range and identifying the relative stability of the three disordered states possible for inverse structures is complex and labor intensive.[97]

Fortunately, there is abundant experimental data for $Mg_8In_{16}S_{32}$, so we simulate cation distributions by using the 56-atom crystallographic unit cell as a template to construct the normal, partial and full inverse orderings, shown as (a), (b) and (c), respectively in Figure 4. All structures started with an approximate $Fd\bar{3}m$ symmetry prior to fully-relaxation.

A. Mg Normal Spinel Structure

The heretofore unobserved *normal*-type $Mg_8In_{16}S_{32}$ is the structure available from crystallographic databases

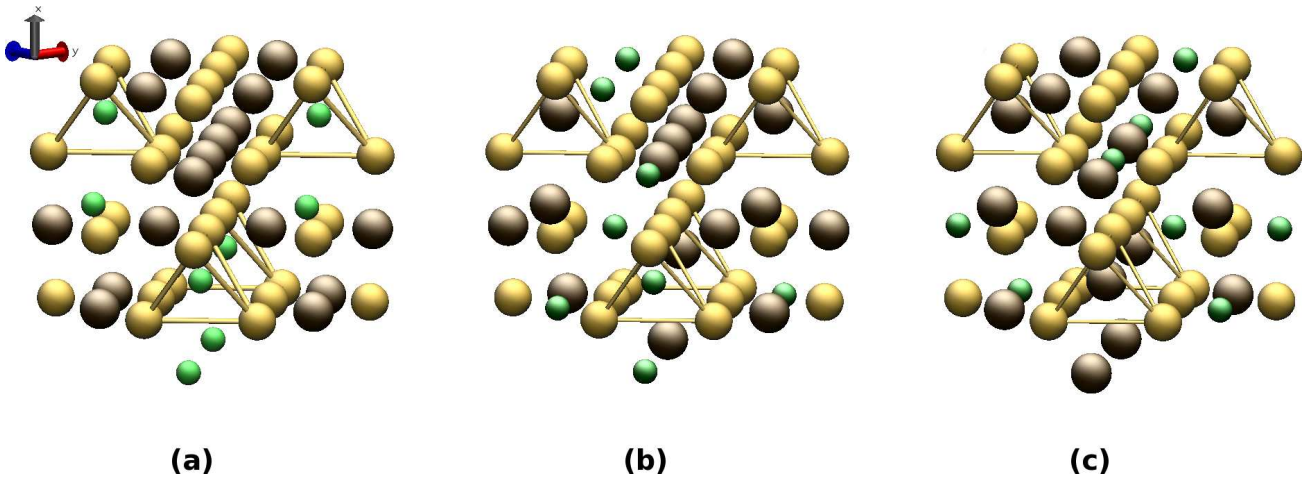

FIG. 4. The three 56-atom conventional, crystallographic unit cells addressing cation ordering for $Mg_8In_{16}S_{32}$ in this study: the (a) **Normal**, (b) **Partial Inverse** and (c) **Full Inverse** spinel structures. The Mg^{+2} cation is green, In^{+3} is brown and the S^{-2} anion is yellow. Cations in T_d holes are surrounded by yellow tetrahedra.

and it is also the easiest to benchmark computationally. The results of several theoretical studies,[61,73,98,99] also provide an alternate means for comparison in the absence of experimental data. The DFT predictions are summarized in Table III.

TABLE III. Normal $Mg_8In_{16}S_{32}$: Functional Dependence of Band Gap (eV) and Lattice Parameters (Å)

Functional (fnl)	LDA		PBE		TPSS		HSE	
Nature of Gap	E_i	E_d	E_i	E_d	E_i	E_d	E_i	E_d
$Mg_8In_{16}S_{32}$								
Experiment	**$a_o = 10.687$**[a]							
a_o	10.715		10.935		10.898		10.840	
Band Gap[b]	1.73		1.69		2.01		2.83	
rlx→HSE$_{sp}$[d]	2.88		2.63		2.71		—-	

[a] ICSD ID 59551.[72]
[b] Fully-relaxed geometry and forces.
[c] Energy calculation of unrelaxed crystal structure.
[d] HSE energy calculation of fullly-relaxed structure.

Paralleling the Cd system, all functionals produce fully-relaxed $Mg_8In_{16}S_{32}$ cells with *expanded* lattice parameters, LDA deviating the least. The band gap is observed to increase as the the cation ordering approaches the normal extreme for the analogous oxide,[81,100] and the Cd thiospinel also followed this pattern, so it is reasonable to expect the Mg *normal* spinel will also have a larger gap. The experimentally-observed band gaps for the Mg system correspond to what is known to be a partial inverse configuration (see Table V) implying that the normal band gap should be *larger* than 2.1-2.3 eV. In fact, HSE predicts a band gap of 2.83 eV – similar in magnitude to the high end 2.7 eV of reported Cd thiospinel gaps. The three semilocal functionals all produce smaller gaps, thus: HSE > TPSS > LDA > PBE. Whether one references the smaller partial inverse measured gaps or trusts the larger HSE prediction paralleling the Cd system (Table I.), errors are on the order of 20-30%.

This data indicates again that the presence of non-local Hartree-Fock exchange in the calculation far out-weighs any lattice differences: indeed, LDA predicts the smallest relaxed volume as well as the narrowest gap, whereas TPSS has a much larger a_o, yet still fails to produce a band gap of the magnitude predicted by HSE and PBE has the largest cell, but the smallest band gap. The HSE single point calculations on the structures relaxed using semilocal functionals provides larger gaps, all within ca. 0.2 eV of the HSE prediction.

Comparison of the normal spinel PDOS for the four functionals is presented in the column to the far left of Figure 5. Again paralleling the Cd thiospinel, the valence band is dominated by the sulfur 3*p*-orbitals, with minor contributions from the indium 5*p*- and 4*d*-orbitals. The conduction band is also dominated by indium 5*s*- and sulfur 3*p*-orbitals in nearly equal amounts. The population patterns remain more or less the same, and a blue shift is again evident. *Unlike* the Cd system, there is no extra structure observed at the edge of the low energy tail of the conduction band, and all four functionals predict that the band gap is *direct*. Nevertheless, a normal spinel structure for $Mg_8In_{16}S_{32}$, has yet to be isolated, so the HSE band gap of 2.83 is purely predictive.

B. Mg Full Inverse Spinel Structure

A fully inverse structure is also unobserved in nature or synthetically, but serves as a close approximation to experiment ($x = 1$ *vs.* $x = 0.84$) facilitating direct comparison. As is evident from Table IV, all functionals predict an*indirect* band gap; the semilocal functions severely underestimate the gap, while HSE yields a 1.98 eV slightly below the experimental range of 2.1-2.3 eV, which is

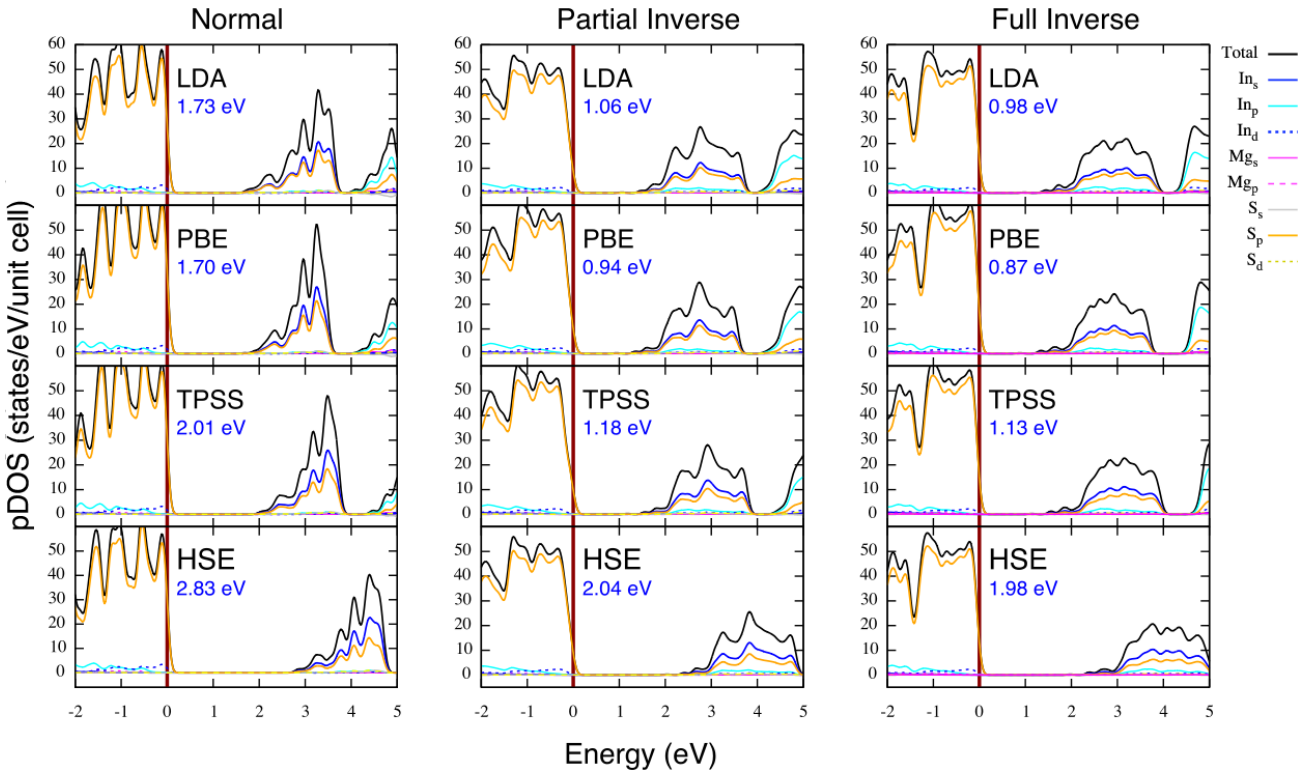

FIG. 5. Projected density of states for $Mg_8In_{16}S_{32}$ for the **Normal**, **Partial Inverse** and **Full Inverse** spinel structures as calculated using LDA, PBE, TPSS and HSE. The Fermi level is indicated by the dark red line at $E = 0$. The top of the valence band does not terminate exactly at zero due to a 10 meV Gaussian line-broadening.

reasonable given that the partial inverse gap should be larger. LDA predicts a slightly contracted lattice, analogous to what is observed for the Cd analog, while all other functionals predict an expansion. The HSE lattice parameters again show the smallest increase in volume.

TABLE IV. Full Inverse $Mg_8In_{16}S_{32}$: Functional Dependence of Band Gap (eV) and Lattice Parameters (Å).

Functional	LDA		PBE		TPSS		HSE	
Nature of Gap	E_i	E_d	E_i	E_d	E_i	E_d	E_i	E_d
$Mg_8In_{16}S_{32}$								
Experiment	**2.1-2.3**[a]			**$a_o = 10.687$**[a]				
a	10.6742		10.9036		10.8665		10.802	
b	10.6801		10.9100		10.8729		10.809	
c	10.6772		10.9056		10.8686		10.804	
Band Gap[b]	0.98	1.04	0.87	0.91	1.13	1.18	1.98	2.04

[a] ICSD ID 59551,[72] with 8 Mg and 8 In exchanged.
[b] Fully-relaxed (geometry and forces) 56-atom cells.

Cursory visual inspection reveals several striking contrasts in both the shape and populations of the calculated PDOS in Figure 5 for the normal (far left) and full inverse (far right) thiospinels. In the normal configuration, the valence band has considerable structure, which is drastically attenuated in the full inverse motif. As with the Cd compounds, the normal spinel conduction band has a slowly diminishing tail and a maximum near the high energy edge of the conduction band, whereas the full inverse conduction band has a more symmetrical population density and an overall smoother "band-shape." In general, both structure-types exhibit similar contributions from the sulfur 3*p*- (yellow) and indium 4*d*-orbitals (blue). However, the indium 5*p*-orbitals (cyan), observed primarily in the valence band of the normal spinel, also show a non-negligible presence in the *conduction* band of the full inverse spinel. This increased In 5*p* contribution can be considered a migration from the high energy band beginning at ca. 4 eV (LDA) in the normal structure, into the lower energy conduction band of the full inverse structure. Finally, the magnesium 3*s*-orbitals (magenta), are seen to contribute – albeit marginally – to both the valence and conduction bands for full-inverse ordering, while not at all, at least in the bands of relevance to the gap, for normal ordering. These dramatic changes in population densities are evident for HSE as well as the semilocal functionals – the main distinction being the increasingly wider band gaps.

C. Partial Inverse Spinel Structure

Most characterizations of synthetic $Mg_8In_{16}S_{32}$ report a *partial inverse* structure.[58,60,101–105] An intermediate

degree of inversion for the 56-atom, full *fcc* conventional unit cell $Mg_8In_{16}S_{32}$ was obtained by taking the structure of Hahn[72] and swapping six cations. Specifically, two In^{3+} are moved from O_h to T_d holes, with four O_h holes swapped with Mg^{2+} "randomly" according to their order in the input file to produced a normality of $x = 0.84$.[102,106] Table V summarizes relevant data for the partial inverse $MgIn_2S_4$ structure. Predictions for the full inverse structure are also included for ease of reference.

TABLE V. Partial Inverse Mg In Thiospinels: Functional Dependence of Band Gap (eV) and Lattice Parameters (Å)

Functional	LDA		PBE		TPSS		HSE	
Nature of Gap	E_i	E_d	E_i	E_d	E_i	E_d	E_i	E_d
$Mg_8In_{16}S_{32}$[a]								
Experiment	**2.1-2.3**[b]				**$a_o = 10.687$**[c]			
a	10.698		10.927		10.889		10.827	
b	10.689		10.919		10.888		10.817	
c	10.694		10.922		10.878		10.822	
Band Gap	1.06	1.08	0.94	0.95	1.18		2.04	2.06
Full Inverse[c]	0.98	1.04	0.87	0.91	1.13	1.18	1.98	2.04

[a] Started with Ref. 72, see text for ordering description, $x \approx 0.84$.
[b] Refs. 58, 61, 102, 103, 105, and 106
[c] ICSD ID 59551, Ref. 72.
[d] $Mg_8In_{16}S_{32}$ from Table IV

As expected, the gaps for full and partial inverse structures are of similar magnitude and the gap is indirect. The semilocal results are underestimate the gap by at least 1 eV, whereas the HSE prediction within 6 meV of the lower bound for the *RT* experimental values of 2.14 eV.[103] Interestingly, low temperature (4 K) experiments indicate an indirect transition across a gap of 2.26 eV, which is 14 meV lower than the direct transition.[104,107] A gap of ca. 2.1 eV suggests that a *partial inverse* structure should be a dark red color, which is, in fact, what is observed.[58,106] This vanishingly small energy difference is also observed in the cubic tin indium thiopinel,[108] several zinc spinels (*e.g.,* $ZnRh_2O_4$[109] or $ZnGa_2O_4$[110]) and the parent β-indium sulfide structure:[74] in all cases, the band gaps are ca. 2-3 eV with a disputed band gap type.

Comparison of both inverse structure PDOSs in Figure 5 (center and right columns), demonstrates the degree of similarity between the partial and full inverse Mg thiospinels. The population densities are similar for both inverse structures and HSE exhibits patterns resembling those produced by the semi-local functionals. Alas, the systems are not identical. Closer examination of the conduction band (HSE) reveals that Mg *s*-orbitals contribute slightly more in the peak of the tail for the partial inverse structure, Figure 6 (top), which is also slightly blue-shifted with respect to the full inverse structure, Figure 6 (bottom), where Mg *p*-orbitals begin to contribute. This enlargement demonstrates that there is also generally more Mg *s*- and *p*-orbital contribution in the conduction band for the full inverse structure. At higher energies, the partial inverse structure shows red-shifted indium *p*-, *d*- and sulfur *s*-orbitals. and noticeable orbital-ordering-by-contribution differences occur at 2.5, 2.9 and 3.0 eV in the conduction band. Note that there is no such contribution in the normal spinel configuration as there is no additional structure at the bottom of the conduction band and the Mg contribution (left column, Figure 5) is primarily at the higher end of the conduction band, not near the band gap.

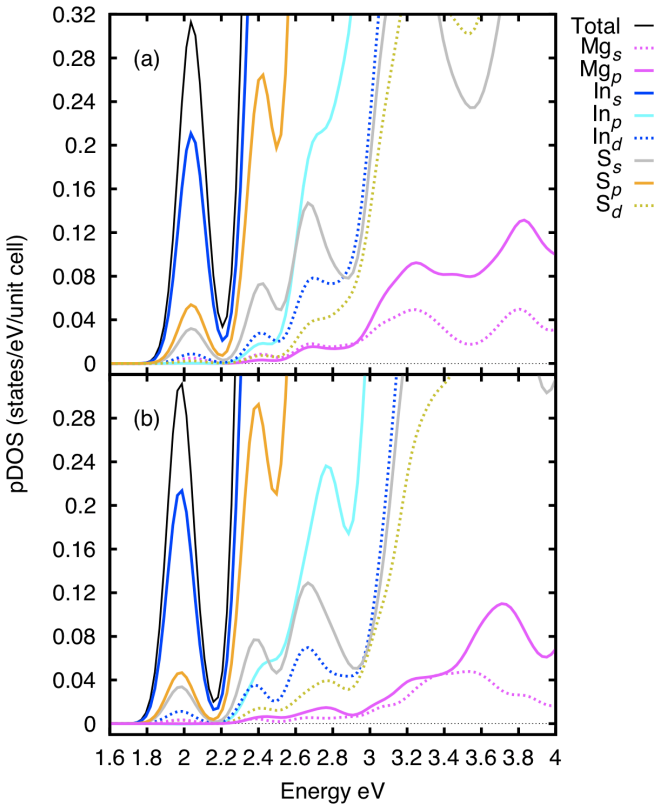

FIG. 6. HSE projected density of states for $Mg_8In_{16}S_{32}$ for the (a) **Partial Inverse** and (b) **Full Inverse** spinel structures. The bottom of the conduction band is enlarged to illustrate dissimilar population patterns. Each plot uses 10 meV Gaussian line-broadening.

The spinel systems are clearly disordered systems.[29,93] When the shape of the optical absorption edge is exponential, producing "Urbach tails,"[111] information about the degree of disorder can be inferred. In recent investigations of the disorder in α-silicon,[112] the calculated DOS and fitting for tails bear striking resemblance to what is observed in spinels.[58] While the valence band in all Cd/Mg thiospinels is sharply terminated, the conduction band has exponential tails. The inverse structures are necessarily more disordered while the normal Cd thiospinel would be more disordered than the unknown Mg analog (which shows no extra band) because of the larger cation.

V. MANY-BODY CALCULATIONS OF THIOSPINELS

The 14-atom $M^{+2}In_2S_4$ primitives for Cd and Mg were relaxed using LDA. Corrected band gaps for the normal Cd, normal Mg and full inverse spinel structures were obtained using a scCOHSEX+G_0W_0 many-body treatment (see Section II.) Symmetry considerations require a 56-atom unit cell for the partial inverse structure, which is not computationally-feasible for scGW, but as was shown previously, properties of the intermediate structure can be inferred from the behavior of the the limiting structures, particularly that of the full inverse structure. The Fermi level is taken to be zero in all plots. For comparison, the same primitives were optimized using HSE.

The resulting band structures are presented in Figure 7, with the scGW and HSE bands on top and bottom, respectively. It is immediately evident that the scGW and HSE band structures are very similar. Further, all calculated band structures, regardless of ordering, exhibit a flat, non-disperse character in the valence band and exhibit a high degree of structure in the conduction band – a pattern typically observed for spinel oxides.[113–115]

In the conduction band, the Cd and Mg cations adopting the normal configuration (left and right columns of Figure 7) display slightly different structure than those of the Mg full inverse ordering (center column), particularly along the $\mathbf{W} \rightarrow \mathbf{K}$ path, where the bands show less curvature, notably around $\mathbf{L}$. It is interesting that the *experimentally-observed* Cd normal (right) and Mg inverse (center) structures manifest similar curvature at the bottom of the conduction band, with a clear separation of the In 5*s*- and slightly higher in energy S 3*s*-orbitals. In contrast, the same bands of the unobserved Mg normal compound (Figure 7 (c) and (e)) overlap.

In terms of band gaps, both scGW and HSE predict an *indirect* transition for the normal Cd compound (Figure 7-(a) and (d), respectively.) The scGW correction locates the valence band maximum along the $\mathbf{K} \rightarrow \mathbf{\Gamma}$ path yielding an indirect gap of 2.98 eV, while HSE predicts a gap of 2.33 eV along the same path.

For the full inverse Mg compound, scGW predicts an *indirect* transition, spanning a 3.04 eV gap that originates from the valence band maximum in the $\mathbf{K} \rightarrow \mathbf{\Gamma}$ direction. The scGW gap is overestimated by ca. 1 eV relative to experiment (Table VI) and the flat top of the valence band conceals the fact that indirect gap is only 10 meV lower than the direct transition. On the other hand, the smaller HSE band gap underestimates experiment by only ca. 0.3 eV. While the HSE prediction is somewhat lower than the experimental range for a *known* partial inverse structure, this is to be expected – the scGW error would also be expected to decrease slightly if a true partial inverse, not a full inverse structure was examined. The small energetic distinction between indirect and direct gaps does not exist for HSE, nor any of the the DFT calculations, when using the smaller, 14-atom primitives, as it did for the 56-atom conventional cells (Tables III and IV), which is not surprising considering the magnitude of $\Delta E_{dir} - E_{ind}$ and the reduction of information inherent to use of a smaller system with fewer electrons.

TABLE VI. Normal and Full Inverse $Mg_2In_4S_48$: scGW Band Gaps (eV) Compared to Four Functionals

Functional (fnl)	LDA		PBE		TPSS		HSE	
Nature of Gap	E_i	E_d	E_i	E_d	E_i	E_d	E_i	E_d
Cd Normal								
Expt	2.2-2.7[a]							
Band Gap[b]	1.34	1.43	1.21	1.30	1.52	1.59	2.33	2.41
scGW[c]	2.98	3.10						
Mg Normal								
Band Gap[d]	1.75		1.69		2.01		2.84	
scGW[c]	3.85							
Mg Full Inverse								
Expt	**2.1-2.2**[e]							
Band Gap[d]	0.96		0.85		1.12		1.93	
scGW[c]	3.04	3.05						

[a] Fully-relaxed 14-atom cells. ICSD ID 300725.[72]
[b] Refs. 52, 57–66
[c] 14-atom *Normal* spinel cell, initially relaxed using LDA.
[d] ICSD ID 59551.[72]
[e] Using partial inverse structure data: Refs. 58, 61, 102, 103, 105, and 106

In the last case, the purely theoretical Mg normal structure, scGW predicts a direct band gap with a magnitude of 3.85 eV. HSE also predicts a direct transition, but the band gap is narrower at 2.84 eV. Nevertheless, the scGW and HSE bands strongly resemble each other (right column of Figure 7.) As there is no experimental data for comparison these gaps remain exclusively predictive, but the HSE band gap is, as was pointed out earlier (see Section IV A) very reasonable.

A. Discussion

For the known Cd and Mg compounds, the difference between experiment and scGW is opposite in sign, but nearly equal in magnitude to the error LDA and GGA typically show for these systems.[73,99] While the scGW scheme used in this work is known to overestimate indirect semiconductor band gaps,[116] the ca. 1 eV disparity for is somewhat larger than the expected 0.1-0.3 eV.[11] There are, however, numerous factors (beyond the precision of the method itself) with the potential to create this large disparity between scGW predictions and experimental measurements.

The most likely issue is probably the neglect of excitonic effects: in medium-gap materials, screening is lower and the electron-hole interaction becomes stronger.[117] Although there is no clear experimental evidence supporting the presence an excitonic effect, the absorption spectra of Ruiz-Fuertes *et al.*[58] might support this hypothesis. Polaronic effects, which are also absent in scGW[14] methods and also show some dependence upon

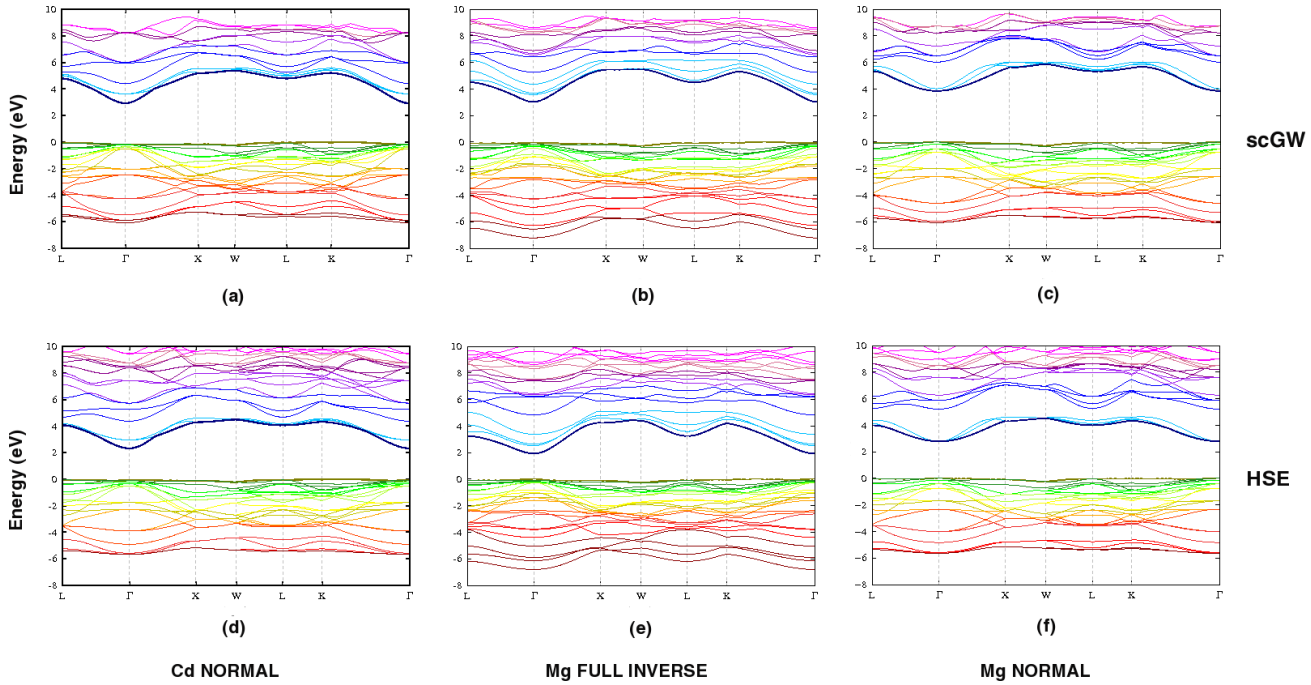

FIG. 7. Comparison of scGW (top) and HSE (bottom) band structures for the Cd/Mg indium thiospinels along the **L Γ X W K Γ** path. **Normal** $Cd_2In_4S_8$ spinel (a) and (d); **Full Inverse** $Mg_2In_4S_8$ spinel, (b) and (e) and the *predicted* Normal spinel ordering for $Mg_2In_4S_8$, **(**c) and (f).

system[118] may also be relevant. While again unverified experimentally, significant polaronic effects are expected from the large $\epsilon_0 - \epsilon_\infty$ that these spinels present ($\epsilon_0 = 18.8 - 20.74, \epsilon_{infty} = 5.5 - 5.8$ for $MgIn_2S_4$[103,119] and $\epsilon_0 = 18.71, \epsilon_{infty} = 6.49$ for $CdIn_2S_4$.[120]) Recently, Vidal[121] showed that neglecting polaronic effects in many-body approaches can lead to band gaps overestimations of up to 1 eV.

To a lesser extent, the differences between the LDA and the experimental structural parameters (not only the lattice parameter a but also the ratio c/a and the internal anion distortion u); the finite temperature of the experiments; the presence of other types of defects in the experimental samples (like silica[103] or Mg vacancies[119]) may also contribute. The combined contributions of these otherwise small effects may explain why scGW consistently overestimates Cd/Mg indium thiospinels by ca. 1 eV.

Nevertheless, recent reports of the successful application of HSE + G_0W_0 for band structures[122,123] suggest an interesting alternative for future exploration.

VI. CONCLUSION

The indium thiopinels of Mg and Cd were examined by a theoretical treatment consisting of DFT and a scGW many-body corrections to LDA. Investigation into the relative performance of LDA, PBE, TPSS and HSE reaffirms earlier observations that semilocal functionals underestimate the band gaps of these semiconductors, regardless of cation ordering, while demonstrating that the screened hybrid HSE provides band gaps and lattice parameters consistently in excellent agreement with experiment. It is also evident that the predictive power of HSE extends beyond the idealized extrema of normal and full inverse spinel occupancies through successful predictions for an experimentally-observed partial inverse spinel structure.

The DFT calculations also indicate that while LDA geometries are generally considered to be better, overall, spinel-type band gaps are far more sensitive to the amount of non-local Hartree-Fock exchange than they are to pm-scale deviations in the lattice parameters. The projected DOS illustrate that the presence of Hartree-Fock exchange induces a significant blue-shift in the location of the bottom conduction band – regardless of the M^{+2} metal present. For all functionals, the conduction band also exhibits distinctive morphological changes as the degree of inversion increases from normal→ full inverse, indicating population re-distribution to lower states. In the valence band the sulfur *3p*-orbitals provide the dominant contribution, while the conduction band consists primarily of the In *5s*-orbitals, followed closely by the sulfur *3p*-orbitals – a pattern strikingly similar to that of β-In_2S_4.

The scGW analysis of band structures reveals that the method overestimates thiospinel band gaps, relative to both experiment and HSE, yet the structure and dispersion patterns of the scGW bands resemble those for other experimentally-characterized spinel systems, as well as

paralleling the predictions from the more expedient and accurate HSE calculations. Both scGW and HSE predict a minute, meV-scale energetic distinction between indirect and direct transitions that is observed for isolable spinel compounds, regardless of configuration type and irrespective of the identity of the M^{+2} cation. Additionally, the strong agreement between the many-body and screened hybrid band structures implies that the details of reliable spinel band structure might serve as a useful adjunct to experimental determination of cation ordering because the normal and inverse spinels manifest dissimilar band patterns.

Thus, this combined DFT/scGW study confirms that the screened hybrid HSE provides an accurate, computationally efficient means for predicting band gaps for the structurally complex Cd/Mg indium sulfide semiconductors.

ACKNOWLEDGMENTS

The work at Rice was funded by the Department of Energy (Grant DE-FG02-09ER16053) and The Welch Foundation (C-0036). The Spanish effort was supported by the Ministerio de Ciencia y Innovacion: Consolider Ingenio 2010 GENESIS-FV (Grant No. CSD2006-04), FOTOMAT (Grant No. MAT2009-14625-C03-01) and the Comunidad de Madrid NUMACIA 2 project (Grant No. S-2009ENE-1477). The authors thankfully acknowledge the computer resources and technical expertise provided by the Centro de Supercomputación y Visualización de Madrid (CeSViMa) and the Spanish Supercomputing Network.

[1] W. Shockley and H. J. Queisser, J. Appl. Phys., **32**, 510 (1961).
[2] A. Luque and A. Martí, Phys. Rev. Lett., **78**, 5014 (1997).
[3] J. P. Perdew and K. Schmidt (American Institute of Physics, 2001).
[4] G. E. Scuseria and V. N. Staroverov, *Theory and Applications of Computational Chemistry: The First 40 Years* (Elsevier, Amsterdam, 2005).
[5] I. Aguilera, P. Palacios, and P. Wahnón, Thin Solid Films, **516**, 7055 (2008).
[6] R. Lucena, I. Aguilera, P. Palacios, P. Wahnón, and J. C. Conesa, Chem. Mater., **20**, 5125 (2008).
[7] P. Palacios, K. Sánchez, J. C. Conesa, J. J. Fernández, and P. Wahnón, Thin Solid Films, **515**, 6280 (2007), *See also:* U.S. Patent **6444897**.
[8] P. Palacios, P. Wahnón, S. Pizzinato, and J. C. Conesa, J. Chem. Phys., **124**, 014711 (2006).
[9] P. Wahnón and C. Tablero, Phys. Rev. B, **65**, 165115 (2002).
[10] S. V. Faleev, M. van Schilfgaarde, and T. Kotani, Phys. Rev. Lett., **93**, 126406 (2004).
[11] F. Bruneval, N. Vast, and L. Reining, Phys. Rev. B., **74**, 045102 (2006).
[12] L. Hedin, Phys. Rev., **139**, A796 (1965).
[13] J. Vidal, S. Botti, P. Olsson, J.-F. Guillemoles, and L. Reining, Phys. Rev. Lett., **104**, 056401 (2010).
[14] J. Vidal, F. Trani, F. Bruneval, M. A. L. Marques, and S. Botti, Phys. Rev. Lett., **104**, 136401 (2010).
[15] M. Gatti, F. Bruneval, V. Olevano, and L. Reining, Phys. Rev. Lett., **99**, 266402 (2007).
[16] F. Bruneval, N. Vast, L. Reining, M. Izquierdo, F. Sirotti, and N. Barrett, Phys. Rev. Lett., **97**, 267601 (2006).
[17] I. Aguilera, *Optoelectronic Characterization by Advanced Ab-Initio Methods of Novel Photovoltaic Intermediate Band Materials.*, Ph.D. thesis, Universidad Politécnica de Madrid (2010), http://oa.upm.es/3669/.
[18] M. van Schilfgaarde, T. Kotani, and S. Faleev, Phys. Rev. Lett., **96**, 226402 (2006).
[19] T. M. Henderson, A. F. Izmaylov, G. Scalmani, and G. E. Scuseria, J. Chem. Phys., **131**, 044108 (2009).
[20] A. V. Krukau, O. A. Vydrov, A. F. Izmaylov, and G. E. Scuseria, J. Chem. Phys., **125**, 224106 (2006).
[21] J. Heyd, G. E. Scuseria, and M. Ernzerhof, J. Chem. Phys., **118**, 8207 (2003).
[22] A. Stroppa, G. Kresse, and A. Continenza, Phys. Rev. B., **83**, 085201 (2011).
[23] A. F. Izmaylov, E. N. Brothers, and G. E. Scuseria, J. Chem. Phys., **125** (2006); J. Heyd, J. E. Peralta, G. E. Scuseria, and R. L. Martin, *ibid.*, **123**, 174101 (2005); J. Heyd and G. E. Scuseria, *ibid.*, **120**, 7274 (2004); **121**, 1187 (2004).
[24] J. Pohl and K. Albe, J. Appl. Phys., **108**, 023509 (2010).
[25] B. G. Janesko, T. M. Henderson, and G. E. Scuseria, Phys. Chem. Chem. Phys., **11**, 443 (2009).
[26] E. N. Brothers, A. F. Izmaylov, J. O. Normand, V. Barone, and G. E. Scuseria, J. Chem. Phys., **129**, 011102 (2008).
[27] 2008 Featured Articles: (a) July 31, "Solar Cell Material Can Soak Up More Sun," http://www.newscientist.com (b) A ugust 9, "A Step Closer to a Next Generation of Solar Cells," http://technology4life.wordpress.com (c) September 30, Technical Insights Report " Intermediate-Band Materials for Solar Cells," Profile of the work done on indium sulfide-based materials. www.frost.com.
[28] T. F. W. Barth and E. Posnjak, Z. Kristallogr., **82**, 325 (1932).
[29] K. E. Sickafus and J. M. Wills, J. Am. Ceram. Soc., **82**, 3279 (1999).
[30] E. J. W. V. amd E. L. Heilmani, J. Chem. Phys., **15**, 174 (1947).
[31] K. N. Kudin and G. E. Scuseria, Phys. Rev. B, **61**, 16440 (2000).
[32] K. N. Kudin and G. E. Scuseria, Chem. Phys. Lett., **289**, 611 (1998).
[33] K. N. Kudin and G. E. Scuseria, Chem. Phys. Lett., **283**, 61 (1998).
[34] M. J. Frisch, G. W. Trucks, H. B. Schlegel, G. E. Scuseria, M. A. Robb, J. R. Cheeseman, G. Scalmani, V. Barone, B. Mennucci, G. A. Petersson, H. Nakatsuji, M. Caricato, X. Li, H. P. Hratchian, A. F. Izmaylov, J. Bloino, G. Zheng, J. L. Sonnenberg, M. Hada, M. Ehara, K. Toyota, R. Fukuda, J. Hasegawa, M. Ishida, T. Nakajima, Y. Honda, O. Kitao, H. Nakai, T. Vreven, J. A. Montgomery, Jr., J. E. Peralta, F. Ogliaro, M. Bearpark, J. J. Heyd, E. Brothers, K. N. Kudin, V. N. Staroverov, R. Kobayashi, J. Normand, K. Raghavachari, A. Rendell, J. C. Burant, S. S. Iyengar, J. Tomasi, M. Cossi, N. Rega, J. M. Millam, M. Klene, J. E. Knox, J. B. Cross, V. Bakken, C. Adamo, J. Jaramillo, R. Gomperts, R. E. Stratmann, O. Yazyev, A. J. Austin, R. Cammi, C. Pomelli, J. W. Ochterski, R. L. Martin, K. Morokuma, V. G. Zakrzewski, G. A. Voth, P. Salvador, J. J. Dannenberg, S. Dapprich, A. D. Daniels, O. Farkas, J. B. Foresman, J. V. Ortiz, J. Cioslowski, and D. J. Fox, "Gaussian 09 Revision A.1," Gaussian Inc., Wallingford CT 2009.
[35] R. Dennington II, T. Keith, and J. Millam, "GaussView 5.0," Semichem, Inc., 2000-2008 Wallingford, CT.
[36] W. Humphrey, A. Dalke, and K. Schulten, J. Mol. Graphics, **14**, 33 (1996), VMD – Visual Molecular Dynamics, version 1.8.7.
[37] See EPAPS Document No. for modified basis sets, information about pseudopotential generation and high graphics of the 56-atom unit cells. For more information on EPAPS, see http://www.aip.org/pubservs/epaps.html.
[38] ICSD, "Inorganic Crystallographic Structural Database," www.fiz-karlsruhe.de/icsd_web.html (2010).
[39] K. N. Kudin, G. E. Scuseria, and H. B. Schlegel, J. Chem. Phys., **114**, 2919 (2001).
[40] J. P. Perdew and Y. Wang, Phys. Rev. B, **45**, 13244 (1992).
[41] S. H. Vosko, L. Wilk, and M. Nusair, Can. J. Phys, **58**, 1200 (1980).
[42] J. P. Perdew, K. Burke, and M. Ernzerhof, Phys. Rev. Lett., **77**, 3865 (1996).
[43] J. P. Perdew, K. Burke, and M. Ernzerhof, Phys. Rev. Lett., **78**, 1396 (1997).
[44] J. Tao, J. P. Perdew, V. N. Staroverov, and G. E. Scuseria, Phys. Rev. Lett., **91**, 146401 (2003).
[45] Specifically, we use the HSEh parameterization[19] of HSE06[20,21], called by the GAUSSIAN keyword HSEh1PBE.

[46] X. Gonze, B. Amadon, P.-M. Anglade, J.-M. Beuken, F. Bottin, P. Boulanger, F. Bruneval, D. Caliste, R. Caracas, M. Cote, T. Deutsch, L. Genovese, P. Ghosez, M. Giantomassi, S. Goedecker, D. R. Hamann, P. Hermet, F. Jollet, G. Jomard, S. Leroux, M. Mancini, S. Mazevet, M. J. T. Oliveira, G. Onida, Y. Pouillon, T. Rangel, G.-M. Rignanese, D. Sangalli, R. Shaltaf, M. Torrent, M. J. Verstraete, G. Zerah, and J. W. Zwanziger, Computer Phys. Commun., **180**, 2582 (2009), ABINIT.

[47] M. Torrent, F. Jollet, F. Bottin, G. Zerah, and X. Gonze, Comput. Mat. Science, **42**, 337 (2008).

[48] G. B. Bachelet, D. R. Hamann, and M. Schluter, Phys. Rev. B, **26**, 4199 (1982).

[49] M. Fuchs and M. Scheffler, Comput. Phys. Commun., **119**, 67 (1999).

[50] M. S. Hybertsen and S. G. Louie, Phys. Rev. B, **34**, 5390 (1986).

[51] R. W. Godby and R. J. Needs, Phys. Rev. Lett., **62**, 1169 (1989).

[52] S. N. Baek, T. S. Jeong, C. J. Youn, K. J. Hong, J. S. Park, D. C. Shin, and Y. T. Yoo, J. Cryst. Growth, **262**, 259 (2004).

[53] H. Nakanishi, Jpn. J. Appl. Phys., **19**, 103 (1980).

[54] S. I. Radustan, V. F. Ihitar, and M. I. Shmiglyuk, Sov. Phys., Semicond., **5**, 1959 (1972).

[55] W. Czaja and L. Krautsbauer, Phys. Stat. Sol., **33**, 191 (1969).

[56] M. R. Brown, M. D. Martin, and W. A. Shand, J. Phys. C: Solid St. Phys., **3**, 1329 (1970).

[57] Y. Li, R. Dillert, and D. Bahnemann, Thin Solid Films, **516**, 4988 (2008).

[58] J. Ruiz-Fuertes, D. Errandonea, F. J. Manjon, D. Martinez-Garcia, A. Segura, V. V. Ursaki, and I. M. Tiginyanu, J. Appl. Phys., **103**, 063710 (2008).

[59] L. Betancourt, V. Sagredo, C. Rincon, and G. E. Delgado, RMxF, **52**, 164 (2006).

[60] S.-J. Lee, J.-E. Kim, and H.-Y. Park, J. Mater. Res., **18**, 733 (2003).

[61] M. Marinelli, S. Baroni, and F. Meloni, Phys. Rev. B, **38**, 8258 (1988).

[62] M. Bohm, G. Huber, A. MacKinnon, and O. Madelung, *Semiconductors Subvolume H: Physics of Ternary Compounds*, Landolt-Bornstein Numerical Data and Functional Relationships in Science and Technology New Series – Group III, Vol. 17 (Springer-Verlag, New York, 1985) and references therein. See p. 137.

[63] G. van Veen and R. D. Beer, J. Phys. Chem. Solids, **38**, 217 (1977).

[64] H. Nakanishi, S. Endo, and T. Irie, J. Phys. Colloques, **36**, C3 (1975), see also Jpn. J. Appl. Phys. 19 (1980) 103.

[65] J. A. Beun, R. Nitsche, and M. Lichtensteiger, Physica, **26**, 647 (1960).

[66] H. Koelmans and H. G. Grimmeiss, Physica, **25**, 1287 (1959).

[67] T. Pisarkiewicz, K. Zakrzewska, and E. Leja, Thin Solid Films, **153**, 479 (1987).

[68] A. J. Nozik, Physical Review B, **6**, 453 (1972).

[69] D. R. Kammler, T. O. Mason, D. L. Young, T. J. Coutts, D. Ko, K. R. Poeppelmeier, and D. L. Williamson, J. Appl. Phys., **90**, 5979 (2001).

[70] E. Burstein, Phys. Rev., **93**, 632 (1954); T. S. Moss, Proc. Phys. Soc. London Sec. A, **382**, 775 (1954).

[71] L. N. Brewer, D. R. Kammler, T. O. Mason, and V. P. Dravid, Journal of Applied Physics, **89**, 951 (2001).

[72] H. Hahn and W. Klinger, Z. Anorg. Allg. Chem., **263**, 177 (1950).

[73] I. Aguilera, P. Palacios, K. Sánchez, and P. Wahnón, Phys. Rev. B, **81**, 075206 (2010).

[74] N. Barreau, A. Mokrani, F. Couzinié-Devy, and J. Kessler, Thin Solid Films, **517**, 2316 (2009).

[75] N. Barreau, Solar Energy, **83**, 363 (2009).

[76] F. Cerrina, C. Quaresima, I. Abbati, L. Braicovich, P. Picco, and G. Margaritondo, Solid State Commun., **33**, 429 (1980).

[77] S. K. Apte, S. N. Garaje, R. D. Bolade, J. D. Ambekar, M. V. Kulkarni, S. D. Naik, S. W. Gosavi, J. O. Baeg, and B. B. Kale, J. Mater. Chem., **20**, 6095 (2010).

[78] L. Schmicka, J. Harl, and G. Kresse, J. Chem. Phys., **134**, 024116 (2011).

[79] E. R. Batista, J. Heyd, R. G. Hennig, B. P. Uberuaga, R. L. Martin, G. E. Scuseria, C. J. Umrigar, and J. W. Wilkins, Phys. Rev. B, **74**, 121102 (2006).

[80] D. O. Scanlon, B. J. Morgan, G. W. Watson, and A. Walsh, Phys. Rev. Lett., **103**, 096405 (2009).

[81] S.-H. Wei and S. B. Zhang, Phys. Rev. B, **63**, 045112 (2001).

[82] M. Womes, J. C. Jumas, and J. Olivier-Fourcade, Solid State Commun., **131**, 257 (2004).

[83] N. Barreau, J. C. Bernède, S. Marsillac, and A. Mokrani, J. Cryst. Growth, **235**, 439 (2002).

[84] G. D. Price, S. L. Price, and J. K. Burdett, Phys. Chem. Miner., **8**, 69 (1982).

[85] U. Schmocker, H. R. Boesch, and F. Waldner, Phys. Lett., **40A**, 237 (1972).

[86] R. J. Hill, J. R. Craig, and G. V. Gibbs, Phys. Chem. Minerals, **4**, 317 (1979).

[87] G. D. Price and N. L. Ross, *The Stability of Minerals*, Mineralogical Society Series, Vol. 3 (Chapman & Hall, New York, 1992).

[88] M. O'Keefe and B. G. Hyde, Struct. Bond., **61**, 71 (1985).

[89] J. C. Deelman, Neues JB Miner. Monat., 289302. (1999).

[90] T. Threlfall, Org. Process Res. Dev., **7**, 1017 (2003).

[91] A. Seko, K. Yuge, F. Oba, A. Kuwabara, and I. Tanaka, Phys. Rev. B, **73**, 184117 (2006).

[92] A. Putnis, *Introduction to Mineral Sciences* (Cambridge University Press, 1992).

[93] A. Seko, F. Oba, and I. Tanaka, Phys. Rev. B, **81**, 054114 (2010).

[94] H. Schmalzried, Z. Phys. Chem., **28**, 203 (1961); J. E. Wiedenborner, N. Stemple, and Y. Okaya, Acta Crystallogr., **20**, 761 (1966).

[95] V. Stevanović, M. dAvezac, and A. Zunger, Phys. Rev. Lett., **105**, 075501 (2010).

[96] A. Seko, K. Yuge, F. Oba, A. Kuwabara, I. Tanaka, and T. Yamamoto, Phys. Rev. B, **73**, 094116 (2006), and references, therein.

[97] A. Zunger, *Statistics and Dynamics of Alloy Phase Transformations* (Plenum, 1992).

[98] F. Semari, R. Khenata, M. Rabah, A. Bouhemadou, S. B. Omran, A. H. Reshak, and D. Rached, J. Solid State Chem., **183**, 2818 (2010).

[99] P. Palacios, I. Aguilera, K. Sánchez, J. C. Conesa, and P. Wahnón, Phys. Rev. Lett., **101**, 046403 (2008).

[100] B. Li, L. Zeng, and F. Zhang, Phys. Stat. Sol. A, **201**, 960 (2004).

[101] V. V. Ursaki, F. Manjón, I. Tiginyanu, and V. E. Tezlevan, J. Phys.: Condens. Matter, **14**, 6801 (2002).

[102] S. Katsuki, Solid State Commun., **39**, 767 (1981).

[103] M. Wakaki, O. Shintani, T. Ogawa, and T. Arai, Jpn. J. Appl. Phys., **19S3**, 255 (1980).
[104] D. Fiorani and S. Viticoli, Sol. State Commun., **32**, 889 (1979).
[105] L. Gastaldi and A. Lapiccirella, J. Sol. State Chem., **30**, 223 (1979).
[106] P. M. Sirimanne, N. Sonoyama, and T. Sakata, J. Solid State Chem., **154**, 476 (2000).
[107] E. Fortin, S. Fafard, A. Anedda, F. Ledda, and A. Charlebois, Solid State Commun., **77**, 165 (1991).
[108] R. Dedryvere, P. E. Lippens, J. C. Jumas, I. Lefebvre-Devos, and C. P. Vicente, Solid State Sci., **3**, 267 (2001).
[109] D. J. Singh, R. C. Rai, J. L. Musfeldt, S. Auluck, N. Singh, P. Khalifah, S. McClure, D. G. Mandrus, W. Shockley, and H. J. Queisser, Chem Mater., **18**, 2696 (2006).
[110] L. Pisani, T. Maitra, and R. Valenti, Phys. Rev. B., **73**, 205204 (2006).
[111] F. Urbach, Phys. Rev., **92**, 1324 (1953).
[112] D. A. Drabold, Y. Li, B. Cai, and M. Zhang, Phys. Rev. B., **83**, 045201 (2011), and references, therein.
[113] W. Setywan and S. Curtarolo, Comp. Mat. Sci., **49**, 299 (2010).
[114] N. Mansourian-Hadavi, S. Wansom, N. H. Perry, A. R. Nagaraja, T. O. Mason, L. H. Ye, and A. J. Freeman, Phys. Rev. B, **81**, 075112 (2010).
[115] S. Lopez, A. H. Romero, P. Rodriguez-Hernandez, and A. Munoz, Phys. Rev. B., **79**, 214103 (2009).
[116] F. Trani, J. Vidal, S. Botti, and M. A. L. Marques, Phys. Rev. B, **82**, 085115 (2010); **83**, 039901(E) (2011).
[117] S. Botti, F. Sottile, N. Vast, V. Olevano, L. Reining, H. C. Weissker, A. Rubio, G. Onida, R. DelSole, and R. W. Godby, Phys. Rev. B, **69**, 155112 (2004).
[118] G. D. Mahan, *Many Particle Physics (Physics of Solids and Liquids)*, 3rd ed. (Springer, 2000) ISBN 978-0306463389.
[119] M. Wakaki, O. Shintani, T. Ogawa, and T. Arai, Jpn. J. Appl. Phys., **21**, 958 (1982).
[120] N. Syrbu, M. Bogdanash, and N. A. Moldovyan, Infrared Physics & Technology, **37**, 763 (1996).
[121] J. Vidal, F. Trani, F. Bruneval, M. A. L. Marques, and S. Botti, Phys. Rev. Lett., **104**, 136401 (2010).
[122] A. Stroppa, M. Marsman, G. Kresse, and S. Picozzi, New Journal of Physics, **12**, 13 (2010).
[123] Y.-S. Kim, K. Hummer, and G. Kresse, Physical Review B, **80**, 035203 (2009).